Journal of Alloys and Compounds 496 (2010) 61–68

Contents lists available at ScienceDirect

Journal of Alloys and Compounds

journal homepage: www.elsevier.com/locate/jallcom

Electronic structure of $FeWO_4$ and $CoWO_4$ tungstates: First-principles FP-LAPW calculations and X-ray spectroscopy studies

S. Rajagopal[a], V.L. Bekenev[b], D. Nataraj[a], D. Mangalaraj[c], O.Yu. Khyzhun[b,*]

[a] Thin Film & Nanomaterials Laboratory, Department of Physics, Bharathiar University, Coimbatore 641 046, India
[b] Frantsevych Institute for Problems of Materials Science, National Academy of Sciences of Ukraine, 3 Krzhyzhanivsky Street, UA-03142 Kyiv, Ukraine
[c] Department of Nanoscience and Technology, Bharathiar University, Coimbatore 641 046, India

ARTICLE INFO

Article history:
Received 2 February 2010
Accepted 10 February 2010
Available online 18 February 2010

Keywords:
Iron tungstate
$FeWO_4$
Cobalt tungstate
$CoWO_4$
Electronic structure
Band structure calculations
X-ray emission spectroscopy
X-ray photoelectron spectroscopy

ABSTRACT

Total and partial densities of states of the constituent atoms of iron tungstate, $FeWO_4$, and cobalt tungstate, $CoWO_4$, have been calculated using the first-principles self-consistent full potential linearized augmented plane wave (FP-LAPW) method. The results obtained reveal that the O 2p-like states are the dominant contributors into the valence band of the tungstates under consideration, whilst the bottom of the conduction band of $FeWO_4$ and $CoWO_4$ is dominated by contributions of the empty Fe 3d- and Co 3d-like states, respectively. The FP-LAPW data indicate that the O 2p-like states contribute mainly into the top of the valence band, with also significant contributions throughout the whole valence-band region, of $FeWO_4$ and $CoWO_4$ compounds. Other significant contributors into the valence-band region are the Fe 3d- and W 5d-like states in $FeWO_4$ and the Co 3d- and W 5d-like states in $CoWO_4$. All the above d-like states contribute throughout the whole valence-band region of the tungstates under consideration, however maximum contributions of the W 5d-like states occur in the lower, whilst the Fe (Co) 3d-like states in the upper portions of the valence band, respectively. To verify the above FP-LAPW data, the X-ray emission bands representing the energy distributions of mainly the valence O p-, Fe (Co) d-, Fe (Co) p- and W d-like states were measured and compared on a common energy scale with the X-ray photoelectron valence-band spectrum of the corresponding tungstate. The experimental data were found to be in good agreement with the theoretical FP-LAPW results for the electronic structure of $FeWO_4$ and $CoWO_4$ compounds.

1. Introduction

Iron tungstate, $FeWO_4$, and cobalt tungstate, $CoWO_4$, belong to a fascinating family of wolframite-type materials which have highly potential and technological applications in many areas such as scintillation detectors, optical fibers, humidity sensors, photoanodes, phase-change optical recording devices, laser hosts, catalysts, pigments, etc. [1–7]. Additionally, wolframite-type tungstates are considered to be novel and commercially important materials due to their several encouraging properties, mainly high values of thermal stability, refractive indexes and X-ray absorption coefficients [8,9]. In particular, among wolframite-type tungstates, $FeWO_4$ and $CoWO_4$ have been intensively studied. $FeWO_4$ and $CoWO_4$ tungstates are well-known p-type semiconductors [10–12]. From experimental measurements [10,13], the energy band gap, E_g, equals 2.8 and 2.0 eV for $CoWO_4$ and $FeWO_4$, respectively. Estimations by Lacomba-Perales et al. [14] based on correlations between the ionic radius of the A^{2+} cation in a number of AWO_4 tungstates reveal values of $E_g = 2.43$ eV for $CoWO_4$ and $E_g = 2.35$ eV for $FeWO_4$. Iron and cobalt tungstates were studied in Refs. [15–18] to explore potential applications of these materials in magnetic fields. As it has been established by Weitzel [15], the magnetic unit cell ($2a,b,c$) of $CoWO_4$ is twice of the chemical unit (a,b,c) and identical with that of $FeWO_4$. Additionally, the magnetic properties of $CoWO_4$ are proved to be symmetric with respect to three orthogonal twofold axes x, y, and z: the 'magnetic' axes x and z are inclined to the vectors a and c of the crystal unit cell at an angle of 40° in the ac-plane, whilst the magnetic axis y lies along the crystal (true) two-fold axis b [16].

$FeWO_4$ and $CoWO_4$ tungstates are isostructural compounds crystallizing in a monoclinic structure belonging to the $P2/a$ space group, with unit cell parameters $a = 4.753$ Å, $b = 5.720$ Å, $c = 4.968$ Å, $\beta = 90.1°$ for $FeWO_4$ [19] and $a = 4.670$ Å, $b = 5.687$ Å, $c = 4.951$ Å, $\beta = 90.0°$ for $CoWO_4$ [20]. The findings by the authors [19,20] are consistent with those derived by other investigators [21–25], as data listed in Table 1 reveal. In the structure of $FeWO_4$ and $CoWO_4$ tungstates, with two formula per unit cell, every metal atom is surrounded by six oxygen atoms: zigzag chains of oxygen octahedra coordinating the metal ions are aligned along the c axis [10]. Iron(cobalt), tungsten and oxygen atoms occupy the 2f, 2e and 4g sites, respectively. As an example, Fig. 1 shows the crystal struc-

* Corresponding author. Tel.: +380 044 424 33 64; fax: +380 044 424 21 31.
E-mail address: khyzhun@ipms.kiev.ua (O.Yu. Khyzhun).

0925-8388/$ – see front matter © 2010 Elsevier B.V. All rights reserved.
doi:10.1016/j.jallcom.2010.02.107

Table 1
Lattice parameters of iron and cobalt tungstates as determined by different authors (monoclinic structure, space group *P2/a*).

Tungstate	Lattice parameters				Reference
	a (Å)	*b* (Å)	*c* (Å)	*β* (°)	
$FeWO_4$	4.753	5.720	4.968	90.1	[19]
$CoWO_4$	4.670	5.687	4.951	90.0	[20]
$CoWO_4$	4.667	5.681	4.947	90.0	[21]
$CoWO_4$	4.666	5.680	4.948	90.0	[22]
$FeWO_4$	4.7289	5.707	4.9630	90.091	[23]
$CoWO_4$	4.9478	5.6827	4.6694	90.0	[24]
$FeWO_4$	4.753	5.720	4.968	90.8	[25]

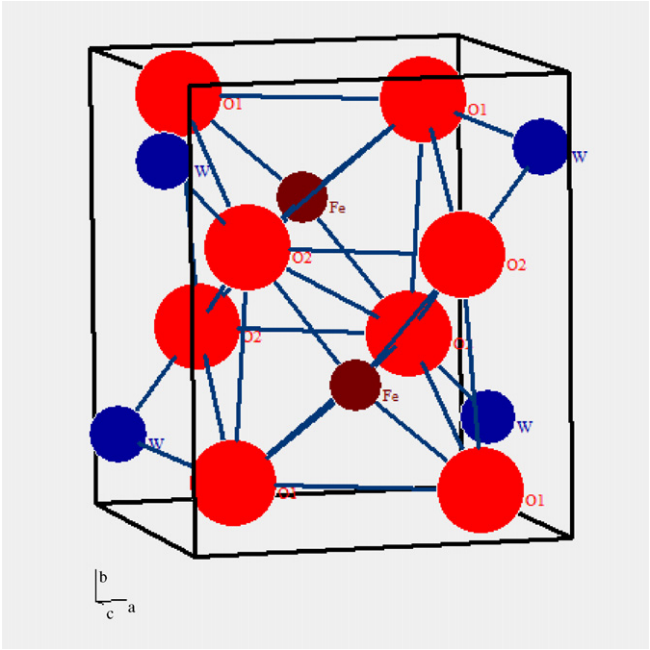

Fig. 1. Crystal structure of iron tungstate, $FeWO_4$: Fe, small brown balls; W, middle blue balls; O, large red balls. (For interpretation of the references to color in this figure legend, the reader is referred to the web version of the article.).

ture of $FeWO_4$. The existence of two non-equivalent positions for oxygen atoms (labelled as O1 and O2; Fig. 1) is characteristic of the structure of $FeWO_4$ and $CoWO_4$ tungstates. There are two tungsten atoms and one iron(cobalt) atom in the nearest arrangement of the O1 atoms, whilst one tungsten atom and two iron(cobalt) atoms are among the nearest neighbours of the O2 atoms [19,20].

Because technological applications of $FeWO_4$ and $CoWO_4$ tungstates are dependent significantly on their quality, different techniques are widely applied for obtaining these compounds in the form of either bulk single crystals (e.g., the flux method [10,13], chemical vapour transport [21]) or polycrystalline materials (e.g., a standard ceramic route [26], the co-precipitation method following by sintering at 500 °C for the formation of a monophasic compound [27]). With the development of nanotechnology, nanostructured transition metal tungstates have attracted much more attention as compared with bulk materials [28,29]. Therefore, $CoWO_4$ nanoparticles were successfully synthesized at a low temperature of 270 °C by a molten salt method [29], by spraying the solution containing $CoCl_2{\cdot}6H_2O$ and $Na_2WO_4{\cdot}2H_2O$ on glass slides at 250–450 °C [7]. Using the same reaction reagents, Zhen et al. [24] have derived single-crystalline $CoWO_4$ nanorods with average diameter of 20 nm and lengths of 100–300 nm using the hydrothermal method, whilst the flower-like hollow cobalt tungstate nanostructures, which consist of $CoWO_4$ nanorods, have been synthesized by alcohol-thermal process at 180 °C employing a simple reaction between $CoCl_2$ and freshly prepared H_2WO_4 in a single alcohol system without any surfactants [30]. Hu et al. [31] have obtained $FeWO_4$ ferberite flowers using mixed $FeCl_3$ and WCl_6 at different ratios in a simple solvo-thermal process adopting cyclohexanol as the solvent. Iron and cobalt tungstate nanostructures, with average sizes of nanoparticles of about 150 and 70 nm in the case of $FeWO_4$ and $CoWO_4$, respectively, have been synthesized very recently in Ref. [32] employing the hydrothermal method and using sodium tungstate ($Na_2WO_4{\cdot}2H_2O$), ferrous ammonium sulfate [$(NH_4)_2Fe(SO_4)_2{\cdot}6H_2O$] and cobalt chloride ($CoCl_2{\cdot}6H_2O$) solutions as precursors.

In a previous article [32], we have reported results of experimental studies of $FeWO_4$ and $CoWO_4$ tungstates employing X-ray photoelectron spectroscopy (XPS), X-ray emission spectroscopy (XES), and X-ray absorption spectroscopy (XAS) methods. The experimental results [32] indicate that the W 5d- and O 2p-like states contribute throughout the whole valence-band region of the $FeWO_4$ and $CoWO_4$ tungstates, however maximum contributions of the O 2p-like states occur in the upper, whilst the W 5d-like states in the lower portions of the valence band, respectively. Nevertheless, to the best of our knowledge, no theoretical band structure calculations have been made so far for $FeWO_4$ and $CoWO_4$. Therefore, in the present article we intend calculating the energy distribution of electronic states of different symmetries of the constituent atoms of iron and cobalt tungstates. With this aim, we have employed possibilities of the full potential linearized augmented plane wave (FP-LAPW) method as incorporated in the WIEN97 code [33] in order to study total density of states (DOS) and partial densities of states of $FeWO_4$ and $CoWO_4$ tungstates. Additionally, some new XES results concerning the energy distribution of the valence states of iron and cobalt in the tungstates under consideration will be reported in the present article.

2. Computational details

Calculations of the electronic structure of $FeWO_4$ and $CoWO_4$ tungstates have been carried out using the first-principles self-consistent FP-LAPW method with the WIEN97 code [33]. In the present FP-LAPW calculations, lattice parameters $a = 4.753$ Å, $b = 5.720$ Å, $c = 4.968$ Å, $\beta = 90.1°$ for $FeWO_4$ and $a = 4.670$ Å, $b = 5.687$ Å, $c = 4.951$ Å, $\beta = 90.0°$ for $CoWO_4$ as well as positions of the constituent atoms of the tungstates under study (Table 2) have been chosen in accordance with the crystallography data determined for the compounds in Refs. [19,20]. For calculations of the exchange-correlation potential, the generalized gradient approximation (GGA) by Perdew et al. [34] has been used. The *muffin-tin*

Table 2
Positions of the constituent atoms of $FeWO_4$ and $CoWO_4$ used in the present FP-LAPW calculations.

Atom	Position of atoms in $FeWO_4$ (Ref. [19])			Position of atoms in $CoWO_4$ (Ref. [20])		
	x	*y*	*z*	*x*	*y*	*z*
Fe(Co)	0.5	0.6785	0.25	0.5	0.6712	0.25
W	0	0.1808	0.25	0	0.1773	0.25
O1	0.2167	0.1017	0.5833	0.2176	0.1080	0.9321
O2	0.2583	0.3900	0.0900	0.2540	0.3757	0.3939

Table 3
Atomic orbitals used in the present FP-LAPW calculations of the electronic structure of $FeWO_4$ and $CoWO_4$.

Atom	Core electrons	Semi-core electrons	Valence electrons	Number of electrons involved in the present FP-LAPW calculations
Fe	$1s^2\ 2s^2\ 2p^6$	$3s^2\ 3p^6$	$4s^2\ 3d^6$	16
Co	$1s^2\ 2s^2\ 2p^6$	$3s^2\ 3p^6$	$4s^2\ 3d^7$	17
W	$1s^2\ 2s^2\ 2p^6\ 3s^2\ 3p^6\ 3d^{10}\ 4s^2\ 4p^6\ 4d^{10}$	$5s^2\ 5p^6\ 4f^{14}$	$5d^4\ 6s^2$	28
O	$1s^2$	$2s^2$	$2p^4$	6

(MT) sphere radii of the constituent atoms in the present calculations were assumed to be as follows: 2.2 a.u. for Fe, 1.95 a.u. for W and 1.60 a.u. for O in the case of $FeWO_4$ and 2.2 a.u. for Co, 1.75 a.u. for W and 1.60 a.u. for O in the case of $CoWO_4$ (1 a.u. = 0.529177 Å). The $R_{min}^{MT}k_{max}$ parameter, where R_{min}^{MT} denotes the smallest MT sphere radius and k_{max} determines the value of the largest k vector in the plane wave expansion, equals 7.0 (the charge density was Fourier expanded up to the value $G_{max} = 15$). The order of a total matrix equals about 1300. In the potential decomposition, the valence wavefunctions inside the MT spheres were expanded up to $l_{max} = 6$. The basis function consists of the atomic orbitals of Fe(Co), W and O as listed in Table 3. In the present calculations, a total number of semi-core and valence electrons (in addition to core electrons) per unit cell equals 136 for $FeWO_4$ and 138 for $CoWO_4$. The tetrahedron method by Blöchl et al. [35] was adopted for integration through the Brillouin zone (BZ). The BZ sampling has been done using 200 k-points within the irreducible wedge of the zone. For calculations of densities of states, an additional sampling was made using 1232 k-points within the irreducible wedge of the BZ. The iteration process was checked taking into account changes of the integral charge difference $q = \int |\rho_n - \rho_{n-1}|\, dr$, where $\rho_{n-1}(r)$ and $\rho_n(r)$ are input and output charge density, respectively. The calculations were interrupted in the case of $q \leq 0.0001$.

3. Experimental

Details of specimens preparation were reported in Ref. [32]. Briefly, $FeWO_4$ and $CoWO_4$ monoclinic tungstates ($P2/a$ space group) with average sizes of nanoparticles of about 150 nm and 70 nm, respectively, were synthesized hydrothermally using sodium tungstate ($Na_2WO_4{\cdot}2H_2O$), ferrous ammonium sulfate [$(NH_4)_2Fe(SO_4)_2{\cdot}6H_2O$] and cobalt chloride ($CoCl_2{\cdot}6H_2O$) solutions as precursors. The products obtained were found to be single-phase materials. XPS and XES measurements [32] have revealed that, the as-prepared $FeWO_4$ and $CoWO_4$ nanostructure tungstates were in a composition close to a stoichiometric one.

The ultrasoft X-ray emission Fe (Co) Lα ($L_{III} \rightarrow M_{IV,V}$ transition) bands reflecting the energy distribution of the valence Fe (Co) s, d-like states in the iron and cobalt tungstates under consideration were measured using an RSM-500 spectrometer. The bands were recorded in the second order of reflection using, as a disperse element, a diffraction grating possessing 600 lines/mm and a radius of curvature of $R \approx 6$ m. The detector was a secondary electron multiplier VEU-6 with a CsI photocathode. Operating conditions of an electron gun in the present experiments were the following: accelerating voltage, $U_a = 5$ kV; anode current, $I_a = 5$ mA. The spectrometer energy resolution was about 0.25–0.3 eV in the energy regions corresponding to the positions of the Fe(Co) Lα bands.

The fluorescent X-ray emission Fe (Co) Kβ$_5$ ($K \rightarrow M_{IV,V}$ transition) bands, which reflect the energy distribution of the valence Fe (Co) p-like states, were derived using a Johann-type DRS-2 M spectrograph equipped with an X-ray BHV-7 tube (gold anode). As a disperse element, a quartz crystal with the $(1\,3\,\bar{4}\,0)$ reflecting plane was used when recording the Fe (Co) Kβ$_5$ bands. Operating conditions of the BHV-7 tube in the experiments were $U_a = 40$ kV and $I_a = 70$ mA. At these experimental conditions, the intensities of the Fe (Co) Kβ$_5$ bands were found to be rather low in $FeWO_4$ and $CoWO_4$: the accumulative time was about 180 h to achieve the sufficient intensities of the bands in the above tungstates. The spectrograph energy resolutions were estimated to be 0.35–0.4 eV when measuring the Fe (Co) Kβ$_5$ bands.

4. Results and discussion

Fig. 2 displays results of the present FP-LAPW band structure calculations of total DOS within a 110-eV range for $FeWO_4$ and $CoWO_4$ tungstates. It is apparent that, the upper core Fe (Co) 3s-, W 5s- and W 4f-like states generate rather narrow bands in $FeWO_4$ and $CoWO_4$, whilst the Fe (Co) 3p- and W 5p-like states form somewhat broader bands in these tungstates. However, the O 2s-like states being among the upper core states generate a rather broad band in the tungstates under consideration with a width of about 2.0 eV (from −15.9 to −17.9 eV) in $FeWO_4$ and about 2.3 eV (from −15.7 to −18.0 eV) in $CoWO_4$. Contributions into the O 2s-like band depend on the positions of oxygen atoms in the lattice of $FeWO_4$ and $CoWO_4$. As one can see from Fig. 3, the dominant contributors into the bottom and the top of the O 2s-like band of $FeWO_4$ are the O1 and O2 atoms, respectively, whilst the both types of oxygen atoms contribute into the central part of the band in almost equal proportions. Further, the bottom and the top of the O 2s-like band of $CoWO_4$ are dominated by contributions of the states associated with the O1 atoms, however the central portion of the band is composed mainly of the O 2s-like states of the O2 atoms. It is worth to mention that first-principles calculations [36–39] also reveal a comparatively wide width (ranging from about 2.0 to 2.4 eV) and a multi-peak structure of the O 2s-like band in a number of MWO_4 tungstates having either the wolframite (M = Cd, Cu, Zn) or scheelite (M = Ca, Pb) structure. The O 2s-like band, with a width of 2.1 eV and

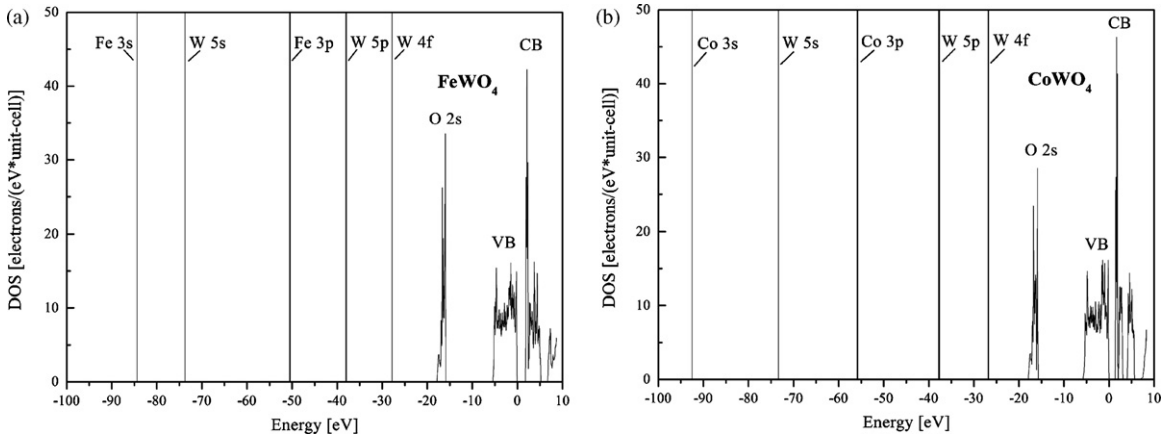

Fig. 2. Plots of total DOS including upper core, valence-band (VB) and conduction band (CB) states of (a) $FeWO_4$ and (b) $CoWO_4$ (*note*: the upper core states are labelled with respect to their dominant atomic contributions).

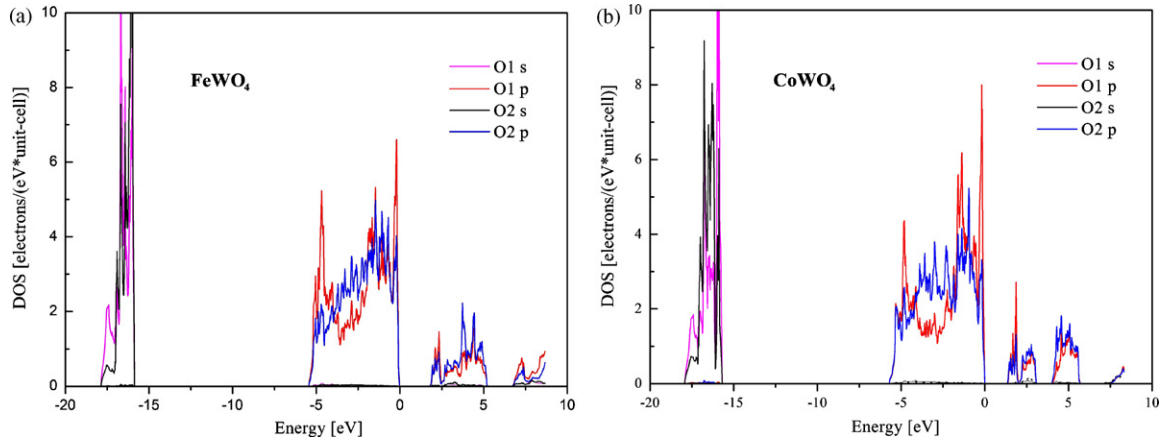

Fig. 3. Partial densities of states of oxygen atoms of (a) $FeWO_4$ and (b) $CoWO_4$.

a number of fine-structure features, was detected very recently in *ab initio* band structure calculations of double $KY(WO_4)_2$ tungstate [40].

Total DOS and total densities of states of the constituent atoms of $FeWO_4$ and $CoWO_4$ tungstates are presented in Fig. 4. The valence band ranges from 0 to −5.45 eV and from 0 to −5.7 eV in the case of $FeWO_4$ and $CoWO_4$, respectively. The present FP-LAPW data are consistent with results of first-principles calculations of other MWO_4 tungstates. As mentioned above, the valence-band width was found to be 5.45 and 5.7 eV in the case of $FeWO_4$ and $CoWO_4$, respectively. These values are comparative to those obtained for valence-band widths of $CaWO_4$ (∼5 eV [36]), $PbWO_4$ (∼5.5 eV [36]), $ZnWO_4$ (∼7.5 eV [38]), and $CuWO_4$ (∼7.7 eV [39]).

As one finds from comparison of Figs. 3 and 4, the O 2p-like states are the dominant contributors to the valence-band region of $FeWO_4$ and $CoWO_4$: the O 2p-like states associated with the O1 atoms contribute mainly into the top and the bottom, whilst the states associated with the O2 atoms into the upper and central portions of the valence band of the tungstates under study. Data of the present FP-LAPW calculations presented in Fig. 4 reveal that tungsten atoms contribute predominantly into the bottom of the valence band of $FeWO_4$ and $CoWO_4$ tungstates, mainly due to contributions of the W 5d-like states, as it is apparent from Fig. 5. Further, iron and cobalt atoms contribute mainly into the upper portions of the valence band of $FeWO_4$ and $CoWO_4$, respectively. Among the electronic states of iron and cobalt atoms, as can be seen from Fig. 6, the Fe 3d- and Co 3d-like states are the principal contributors into the valence-band region of $FeWO_4$ and $CoWO_4$, respectively.

Figs. 3 and 5 render that the strong hybridization of the W 5d- and O1 2p-like states is characteristic for the lower portion of the valence band of the tungstates under consideration. Additionally, the O 2p-like states associated with the O2 atoms are highly hybridized with the Fe 3d- and Co 3d-like states in the upper portion of the valence band of $FeWO_4$ and $CoWO_4$, respectively (cf. Figs. 3 and 6). These FP-LAPW data partly confirm the suggestions by Ejima et al. [13] made on the basis of ultraviolet photoelectron spectroscopy (UPS) studies of $FeWO_4$ that the O 2p- and Fe 3d-like states hybridize and spread wide in the valence band of this tungstate.

Fig. 4 shows that a rather narrow band *a* ranging from 1.78 to 2.45 eV in $FeWO_4$ and from 1.36 to 2.0 eV in $CoWO_4$ can be distinguished at the bottom of the conduction bands of the above tungstates. This band in $FeWO_4$ and $CoWO_4$ tungstates is composed mainly of the empty Fe 3d- and Co 3d-like states, respectively, as data of the FP-LAPW calculations presented in Figs. 4 and 6 reveal. In $CoWO_4$, the band *a* is separated from a somewhat broader upper band *b* by a small gap of about 0.05 eV (Fig. 4b), whilst the band *b* superimposes the band *a* in the case of $FeWO_4$ (Fig. 4a). The origin of the band *b* in the both tungstates under consideration is similar to that of the band *a*: the band *b* is composed mainly of the contributions of the empty Fe 3d- and Co 3d-like states in $FeWO_4$ and $CoWO_4$, respectively (cf. Figs. 4 and 6). Further, the band *b* is separated by a gap of about 0.9 eV from a rather broad upper band *c* in the case of $CoWO_4$, whilst in $FeWO_4$ the band *c* superimposes the band *b* (see Fig. 4). In the both tungstates under study, the main contributors into the band *c* are the empty W 5d- and O 2p-like states, as data presented in Figs. 3–5 reveal.

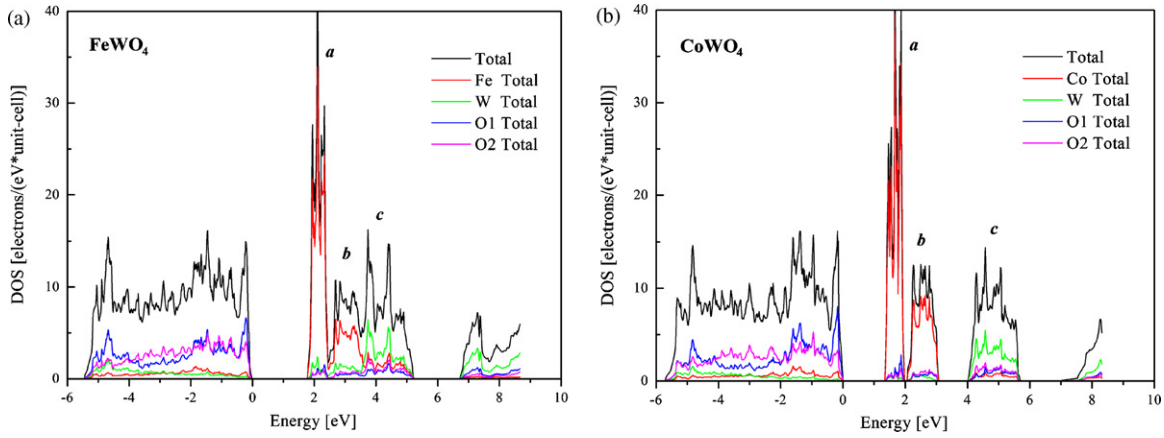

Fig. 4. Total DOS and total densities of states of the constituent atoms of (a) $FeWO_4$ and (b) $CoWO_4$ (within the valence-band and conduction band regions).

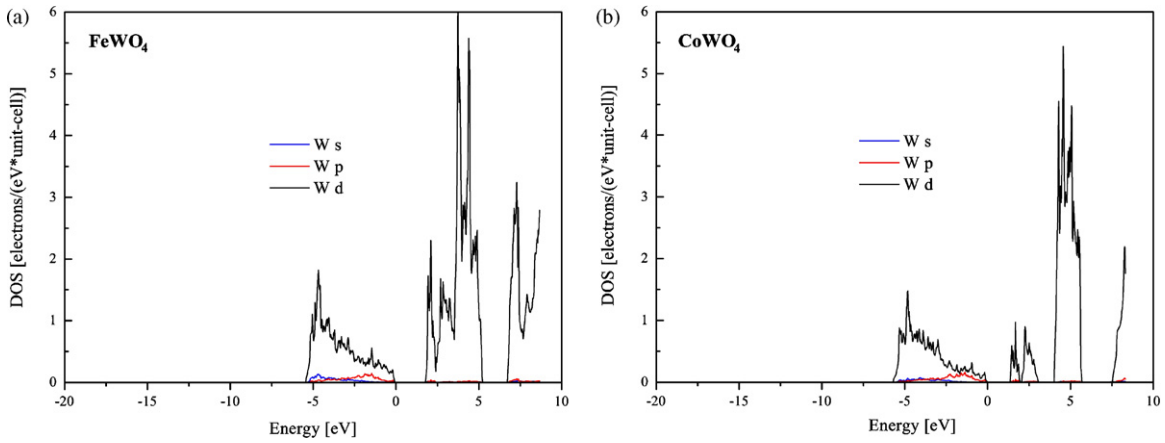

Fig. 5. Partial densities of states of tungsten atoms of (a) $FeWO_4$ and (b) $CoWO_4$ (within the valence-band and conduction band regions).

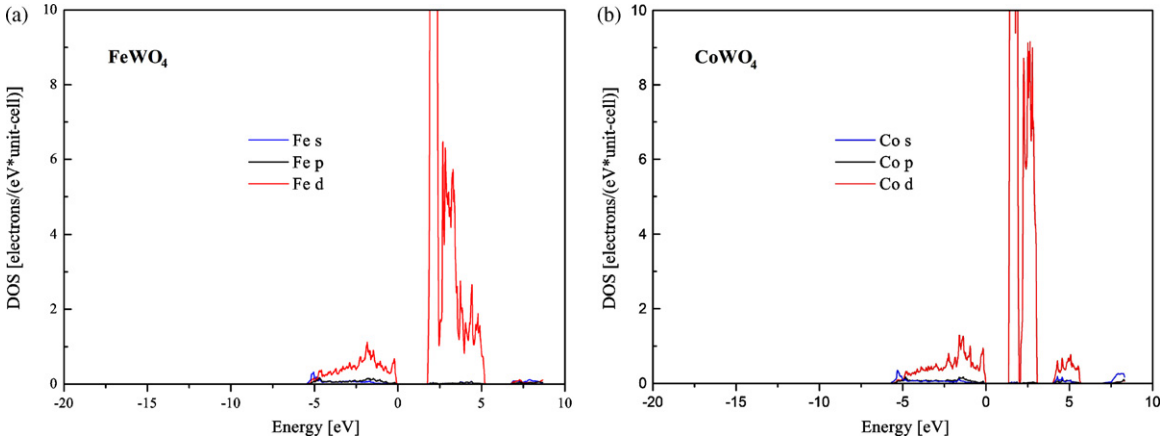

Fig. 6. Partial densities of states of (a) iron atoms of $FeWO_4$ and (b) of cobalt atoms of $CoWO_4$ (within the valence-band and conduction band regions).

From comparison of Figs. 3–6, it is apparent that the contributions of the W 6s-, W 6p-, Fe(Co) 4s-, Fe (Co) 4p- and O 2s-like states are rather minor throughout the valence-band and conduction band regions of $FeWO_4$ and $CoWO_4$ tungstates. Due to the UPS results by Ejima et al. [13], the bottom of the conduction band of $FeWO_4$ is attributed to the empty Fe 4s-like states. As one finds from Fig. 6b, the empty Fe 4s-like states (as well as the remaining iron empty states, mainly Fe 4p and Fe 3d) appear beginning from 1.78 eV and spread towards higher energies. Nevertheless, the contributions of the empty Fe 3d-like states at the bottom of the conduction band of $FeWO_4$ are much higher compared with those of the empty Fe 4s- and Fe 4p-states (see Fig. 6a).

With respect to the valence-band occupations, the present FP-LAPW data for $FeWO_4$ and $CoWO_4$ seem to agree fairly well with the experimental results for these tungstates. The experimental X-ray emission Fe (Co) Lα and Fe (Co) $K\beta_5$ bands recorded for $FeWO_4$ and $CoWO_4$ tungstates are depicted in Fig. 7 on a common energy scale with the X-ray emission W $L\beta_5$ and O Kα bands as well as with the XPS valence-band spectra derived for the tungstates in Ref. [32]. For such a procedure, we have taken into account binding energies of the core-level electrons recorded for the $FeWO_4$ and $CoWO_4$ compounds in Ref. [32] and using measurements of photon energies of suitable inner X-ray lines. The method of matching the X-ray emission bands of $FeWO_4$ and $CoWO_4$ tungstates on a common energy scale was analogous to that used previously when studying the electronic structure of other tungstates [39,40]. From Fig. 7, it is evident that, in agreement with the theoretical band structure data depicted in Figs. 3–6, the main contributions of the W 5d- and Fe (Co) 3d-like states occur in the lower and upper portions of the valence band of $FeWO_4$ ($CoWO_4$), respectively, with the contributions of the mentioned states in the whole valence-band regions of the tungstates studied. Additionally, the experimental data presented in Fig. 7 show that the top of the valence band is dominated by contributions of the O 2p-like states, being in agreement with the FP-LAPW results (cf. Figs. 3 and 4). It is necessary to mention that, in spite of the comparatively small contributions of the valence Fe p- and Co p-like states in the valence-band region of $FeWO_4$ and $CoWO_4$ tungstates, as predicted by the FP-LAPW calculations (Fig. 6), it was possible to obtain in the present work the XES Fe $K\beta_5$ and Co $K\beta_5$ bands, representing the energy distributions of the M 4p-like states in the above MWO_4 tungstates (however, it took rather long accumulative times for recording such spectra as mentioned in the Experimental section). As can be seen in Fig. 7, the X-ray emission Fe $K\beta_5$ and Co $K\beta_5$ bands of $FeWO_4$ and $CoWO_4$, respectively, are rather broad and without fine-structure peculiarities. These results are consistent with the theoretical data presented in Fig. 6. As one can see from this figure, the theoretical curves representing partial densities of the Fe p- and Co p-like states are rather flat, with only two humps at the bottom and in the upper portion of the valence band of the tungstates. These humps are not resolved on the experimental spectra, probably because of the rather broad widths of the K level, mainly about 1.0 and 1.1 eV for iron and cobalt, respectively [41]. Since the X-ray emission Fe (Co) $K\beta_5$ bands are positioned on the high-energy slope of the inner Fe (Co) $K\beta_{1,3}$ lines ($K \rightarrow M_{II,III}$ transition), the above bands are sig-

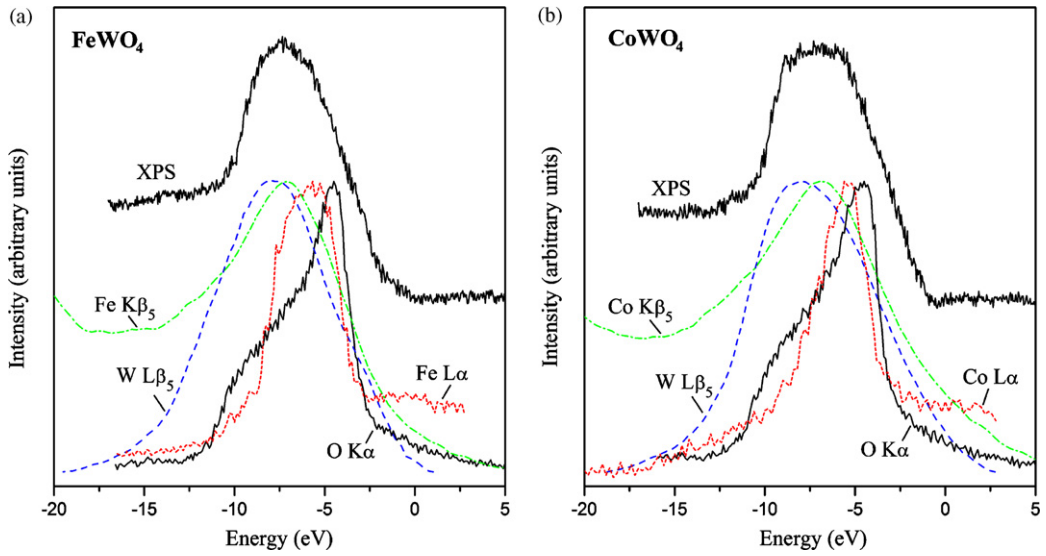

Fig. 7. The X-ray emission Fe (Co) Lα, Fe (Co) $K\beta_5$, W $L\beta_5$ and O Kα bands matched on a common energy scale with the XPS valence-band spectra of (a) $FeWO_4$ and (b) $CoWO_4$ (*note*: the XPS valence-band spectra were excited by Al Kα radiation (E = 1486.6 eV) as reported in Ref. [32]).

nificantly asymmetric in the $FeWO_4$ and $CoWO_4$ tungstates studied (Fig. 7).

It is necessary to indicate that predominant contributions of the W 5d- and O 2p-like states into the lower and upper portions of the valence band, respectively, established for $FeWO_4$ and $CoWO_4$ tungstates, look to be a common peculiarity of the electronic structure of MWO_4 tungstates. In particular, this peculiarity was theoretically detected for $CaWO_4$ and $PbWO_4$ [36,42], $CdWO_4$ [37,43], $ZnWO_4$ [38,44], $CuWO_4$ [39] and $SrWO_4$ [45]. From analysis of the theoretical data for MWO_4 tungstates [36–39,42–45], one can conclude that the region of main contributions of the valence states associated with the M atom depends significantly on its position in the Periodic Table. Additionally, the first-principles band structure and cluster calculations [36–39,42–45] render that the O 2p-like states are the main contributors to the valence band of a number of MWO_4 tungstates (M = Ca, Cd, Pb, Cu, Zn). This conclusion is confirmed by XPS measurements and by theoretical calculations carried out within relativistic molecular orbital and/or discrete variational Xα methods for Pb, Ca, Ba, Cd and Zn tungstates [46,47], by XPS and XES data for $CuWO_4$ [48], by polarized reflectivity spectra for $CaWO_4$ [49].

Further, as mentioned above, the present FP-LAPW calculations predict the increasing width of the valence-band region from 5.45 to 5.7 eV when going from $FeWO_4$ to $CoWO_4$. This prediction is confirmed by the experimental results presented in Fig. 7. From this figure it is apparent that, when going from $FeWO_4$ to $CoWO_4$,

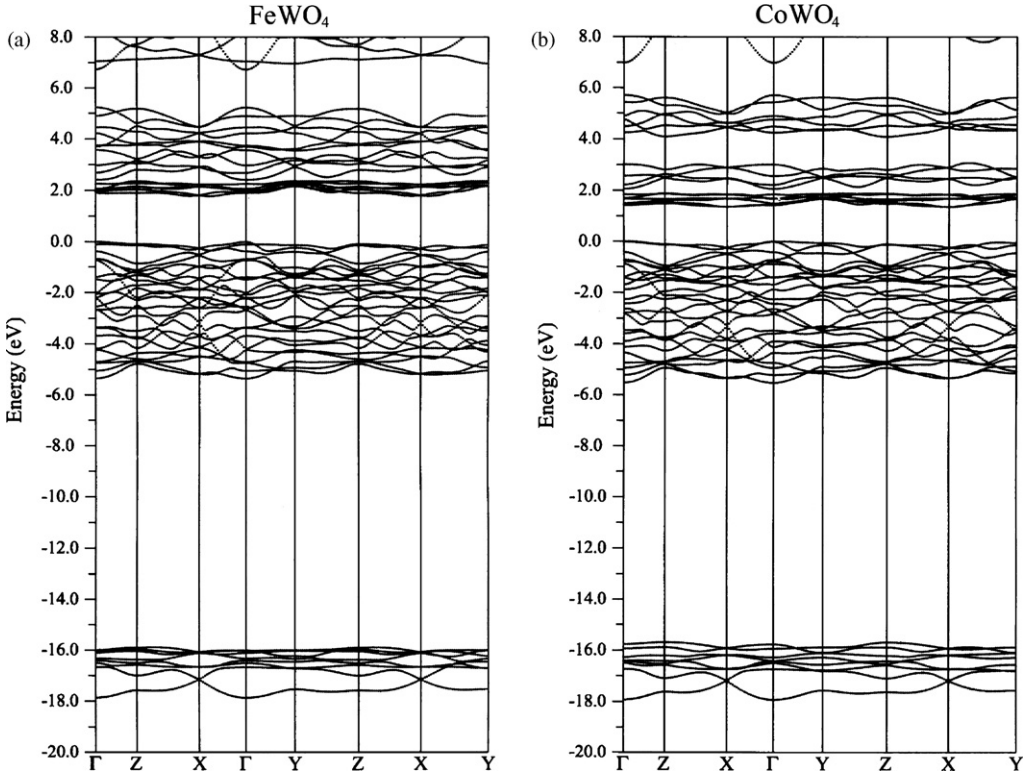

Fig. 8. Electronic bands along selected symmetry paths within the first Brillouin zone of (a) $FeWO_4$ and (b) $CoWO_4$.

the full width at half-maximum (FWHM) of the XPS valence-band spectrum, the XES W $L\beta_5$ and O $K\alpha$ bands increases by 0.45, 0.3 and 0.4 eV, respectively. It is incorrect to compare the FWHM values for the X-ray emission Fe (Co) $L\alpha$ and Fe (Co) $K\beta_5$ bands in $FeWO_4$ and $CoWO_4$ because the energy resolution of the X-ray emission spectrometers equipped with either a grating or a crystal as a disperse element usually depends on a photon energy region [50,51]. In addition, the energy widths of the K and L_{III} levels are different for iron and cobalt [41].

Band dispersions for $FeWO_4$ and $CoWO_4$ tungstates are plotted in Fig. 8 for several symmetry directions of the monoclinic Brillouin zone. The diagram of the monoclinic Brillouin zone used in the present FP-LAPW calculations is analogous to that published previously in Ref. [37]. The coordinates of the *k*-points, within the limited region of the Brillouin zone studied for the band dispersions (Fig. 8), are as follows: Γ (0.0 0.0 0.0), *X* (0.5 0.0 0.0), *Y* (0.0 0.5 0.0), and *Z* (0.0 0.0 0.5). We would like to mention that values of the band gaps of E_g = 1.78 eV for $FeWO_4$ and E_g = 1.36 eV for $CoWO_4$, as band structure diagrams presented in Fig. 8 reveal, are smaller than those measured experimentally [10,13] and estimated by Lacomba-Perales et al. [14] for these tungstates. The values of band gaps calculated within the GGA approximation [33] are known to be underestimated [52,53]. Since the real values of the band gaps of $FeWO_4$ and $CoWO_4$ tungstates, to the best of our knowledge, have not been determined precisely yet [14], we have not made any scissors corrections of the band structure diagrams presented in Fig. 8.

The shapes of the band dispersions for $FeWO_4$ and $CoWO_4$ look very similar to each other, as Fig. 8 displays. The dispersions of the curves near the conduction band minima and valence-band maxima are rather flat for the both tungstates studied. The valence-band maximum for $FeWO_4$ is located at the Γ point at the centre of the Brillouin zone, however the conduction band minimum is positioned away from the Γ point, mainly at k = (0.262 0.0 0.0) in the X–Γ direction. Further, the conduction band for $CoWO_4$ has its minimum at the X point, whilst the valence-band maximum is located in the Γ–Y direction, mainly at k = (0.0 0.015 0.0). The above data allow assuming that, $FeWO_4$ and $CoWO_4$ are indirect-gap materials.

Main features of the valence-band dispersions for $FeWO_4$ and $CoWO_4$ are similar to those for the scheelite- and wolframite-type tungstates studied previously in Refs. [36–39,44]. Nevertheless, due to the LAPW calculations by Zhang et al. [36], a direct band gap at the center of Brillouin zone is characteristic of $CaWO_4$, whilst band extrema for $PbWO_4$ occur at wave vectors away from the zone center (the valence band has maximum in the Δ direction and slightly lower maximum in the Σ direction, but the conduction band minimum is located in the Σ direction). The minimum band gap for $CdWO_4$ was found to occur at the *Y* point located at the center of the Brillouin zone boundary plane, which is perpendicular to the crystal axis [37]. The minimum band gap for $ZnWO_4$, due to *ab initio* calculations by Kalinko et al. [38] employing the periodic linear combination of atomic orbitals (LCAO) method, again occurs at the *Y* point and correspond to a direct transition. The above results indicating a strong influence of a divalent M atom on the electronic structure of MWO_4 tungstates confirm suggestions by Lacomba-Perales et al. [14] based on optical-absorption and reflectance measurements of a number of MWO_4 monocrystals (M = Ba, Ca, Cd, Cu, Pb, Sr, Zn) that electronic properties of these materials depend significantly on the position of the M atom in the Periodic Table.

5. Conclusions

The present first-principles FP-LAPW calculations reveal the similarity of the electronic structure and the band dispersions of monoclinic $FeWO_4$ and $CoWO_4$ tungstates. In these compounds, the dominant contributors into the valence band are the O 2p-like states. The above states contribute mainly into the top of the valence band, with also significant contributions throughout the whole valence-band region. Other significant contributors into the valence-band region of $FeWO_4$ and $CoWO_4$ tungstates are the W 5d- and Fe (Co) 3d-like states. Maximum contribution of the W 5d-like states occur in the lower, whilst those of the Fe (Co) 3d-like states in the upper portions of the valence band of the tungstates under consideration. The FP-LAPW data are confirmed experimentally by comparison on a common energy scale of the X-ray emission bands, representing the energy distributions of mainly the O 2p-, Fe (Co) 3d-, Fe (Co) 4p- and W 5d-like states. Additionally, the FP-LAPW data reveal that contributions of the empty Fe 3d- and Co 3d-like states dominate at the bottom of the conduction band of $FeWO_4$ and $CoWO_4$, respectively.

Acknowledgement

One of the authors, S. Rajagopal would like to thank Bharathiar University for awarding University Research Fellowship to carry out this work.

References

[1] H. Grassmann, H.-G. Moser, E. Lorenz, J. Lumin. 33 (1985) 109–113.
[2] H. Wang, F.D. Medina, D.D. Liu, Y.-D. Zhous, J. Phys. : Condens. Matter 6 (28) (1994) 5373–5386.
[3] A.R. Phani, M. Passacantando, L. Lozzi, S. Santucci, J. Mater. Sci. 35 (2000) 4879–4883.
[4] H. Kraus, V.B. Mikhailik, Y. Ramachers, D. Day, K.B. Hutton, J. Telfer, Phys. Lett. B 610 (2005) 37–44.
[5] Q. Zhang, W.-T. Yao, X. Chen, L. Zhu, Y. Fu, G. Zhang, L. Sheng, S.-H. Yu, Cryst. Growth Des. 7 (2007) 1423–1431.
[6] A.L.M. de Oliveira, J.M. Ferreira, M.R.S. Silva, G.S. Braga, L.E.B. Soledade, M.A.M. Maria Aldeiza, C.A. Paskocimas, S.J.G. Lima, E. Longo, A. Gouveia de Souza, I.M. Garcia dos Santos, Dyes Pigments 77 (2008) 210–216.
[7] S. Thongtem, S. Wannapop, T. Thongtem, Ceram. Int. 35 (5) (2009) 2087–2091.
[8] X. Jiang, J. Ma, J. Liu, Y. Ren, B. Lin, J. Tao, X. Zhu, Mater. Lett. 61 (23–24) (2007) 4595–4598.
[9] G.B. Kumar, K. Sivaiah, S. Buddhudu, Ceram. Int. 36 (2010) 199–202.
[10] R. Bharati, R.A. Singh, B.M. Wanklyn, J. Mater. Sci. 16 (1981) 775–779.
[11] K. Sieber, K. Kourtakis, R. Kershaw, K. Dwight, A. Wold, Mater. Res. Bull. 17 (6) (1982) 721–725.
[12] E. Schmidbauer, U. Schanz, F.J. Yu, J. Phys. : Condens. Matter 3 (28) (1991) 5341–5352.
[13] T. Ejima, T. Banse, H. Takatsuka, Y. Kondo, M. Ishino, N. Kimura, M. Watanabe, I. Matsubara, J. Lumin. 119–120 (2006) 59–63.
[14] R. Lacomba-Perales, J. Ruiz-Fuertes, D. Errandonea, D. Martínez-García, A. Segura, Europhys. Lett. 83 (3) (2008) 37002.
[15] H. Weitzel, Solid State Commun. 8 (24) (1970) 2071–2072.
[16] V.M. Gredescul, S.A. Gredescul, V.V. Eremenko, V.M. Naumenko, J. Phys. Chem. Solids 33 (4) (1972) 859–880.
[17] H. Weitzel, H. Langhof, J. Magn. Magn. Mater. 4 (1977) 265–274.
[18] E. García-Matres, N. Stüßer, M. Hofmann, M. Reehuis, Eur. Phys. J. B 32 (2003) 35–42.
[19] C. Escobar, H. Cid-Dresdner, P. Kittl, I. Dümler, Am. Mineral. 56 (1971) 489–498.
[20] H. Weitzel, Z. Kristallogr. 144 (1976) 238–258.
[21] A.W. Sleight, Acta Cryst. B 28 (1972) 2899–2902.
[22] C.P. Landee, E.F. Westrum Jr., J. Chem. Thermodyn. 8 (1976) 471–491.
[23] F. Yu, U. Schanz, E. Schmidbauer, J. Cryst. Growth 132 (1993) 606–608.
[24] L. Zhen, W.-S. Wang, C.-Y. Xu, W.-Z. Shao, L.-C. Qin, Mater. Lett. 62 (2008) 1740–1742.
[25] Y.-X. Zhou, H.-B. Yao, Q. Zhang, J.-Y. Gong, S.-J. Liu, S.-H. Yu, Inorg. Chem. 48 (2009) 1082–1090.
[26] R.C. Pullar, S. Farrah, N.McN. Alford, J. Eur. Ceram. Soc. 27 (2007) 1059–1063.
[27] S.J. Naik, A.V. Salker, Catal. Commun. 10 (2009) 884–888.
[28] C.-L. Li, Z.-W. Fu, Electrochim. Acta 53 (12) (2008) 4293–4301.
[29] Z. Song, J. Ma, H. Sun, Y. Sun, J. Fang, Z. Liu, C. Gao, Y. Liu, J. Zhao, Mater. Sci. Eng. B 163 (2009) 62–65.
[30] T. You, G. Cao, X. Song, C. Fan, W. Zhao, Z. Yin, S. Sun, Mater. Lett. 62 (2008) 1169–1172.
[31] W. Hu, Y. Zhao, Z. Liu, C.W. Dunnill, D.H. Gregory, W. Zhu, Chem. Mater. 20 (17) (2008) 5657–5665.
[32] S. Rajagopal, D. Nataraj, O.Y. Khyzhun, Y. Djaoued, J. Robichaud, D. Mangalaraj, J. Alloys Compd. 493 (2010) 340–345.
[33] P. Blaha, K. Schwarz, J. Luitz, WIEN97, A Full Potential Linearized Augmented Plane Wave Package for Calculating Crystal Properties, Technical University, Vienna, 1999 (Improved and update Unix version of the original copyrighted WIEN-code, which was published by P. Blaha, K. Schwarz, P. Sorantin, S. B. Trickey, Comput. Phys. Commun. 59 (1990) 399–415).

[34] J.P. Perdew, S. Burke, M. Ernzerhof, Phys. Rev. Lett. 77 (1996) 3865–3868.
[35] P.E. Blöchl, O. Jepsen, O.K. Andersen, Phys. Rev. B 49 (1994) 16223–16233.
[36] Y. Zhang, N.A.W. Holzwarth, R.T. Williams, Phys. Rev. B 57 (1998) 12738–12750.
[37] Y. Abraham, N.A.W. Holzwarth, R.T. Williams, Phys. Rev. B 62 (2000) 1733–1741.
[38] A. Kalinko, A. Kuzmin, R.A. Evarestov, Solid State Commun. 149 (2009) 425–428.
[39] O.Y. Khyzhun, V.L. Bekenev, Y.M. Solonin, J. Alloys Compd. 480 (2009) 184–189.
[40] V.L. Bekenev, O.Y. Khyzhun, V.V. Atuchin, J. Alloys Compd. 485 (2009) 51–58.
[41] M.A. Blokhin, I.G. Shveitser, Handbook on X-Ray Spectra, Nauka, Moscow, 1982.
[42] Z. Yi, T. Liu, Q. Zhang, Y. Sun, J. Electron Spectrosc. Relat. Phenom. 151 (2006) 140–143.
[43] X. Zhou, T. Liu, Q. Zhang, F. Cheng, H. Qiao, Solid State Commun. 150 (2010) 5–8.
[44] H. Fu, J. Lin, L. Zhang, Y. Zhu, Appl. Catal. A 306 (2006) 58–67.
[45] M. Song, Q. Zhang, T. Liu, J. Yin, X. Guo, H. Zhang, X. Wang, Curr. Appl. Phys. 9 (2009) 812–815.
[46] M. Itoh, N. Fujita, Y. Inabe, J. Phys. Soc. Jpn. 75 (2006) 084705.
[47] M. Fujita, M. Itoh, T. Katagiri, D. Iri, M. Kitaura, V.B. Mikhailik, Phys. Rev. B 77 (2008) 155118.
[48] O.Y. Khyzhun, T. Strunskus, S. Cramm, Y.M. Solonin, J. Alloys Compd. 389 (2005) 14–20.
[49] M. Fujita, M. Itoh, S. Takagi, T. Shimizu, N. Fujita, Phys. Status Solidi (B) 243 (8) (2006) 1898–1907.
[50] A. Meisel, G. Leonhardt, R. Szargan, X-Ray Spectra and Chemical Binding, Springer-Verlag, Berlin, Heidelberg, 1989.
[51] E.Z. Kurmaev, V.M. Cherkashenko, L.D. Finkelnstein, X-ray Spectra of Solids, Nauka, Moscow, 1988.
[52] S. Kurth, S. Pittalis, L.D. Finkelnstein, in: J. Grotendorst, S. Blugel, D. Marx (Eds.), The Optimized Effective Potential Method and LDA+ U Computational Nanoscience: Do It Yourself! NIC Series, vol. 31, John von Neumann Institute for Computing, Julich, 2006, ISBN 3-00-017350-1, pp. 299–334.
[53] A.J. Cohen, P. Mori-Sánchez, W. Yang, Phys. Rev. B 77 (2008) 115123-1–1115123-6.